express
polymer letters

Research article

Polyacrylonitrile/bio-based polyurethane electrospun fiber mats as advanced separators for high-performance Zn-ion batteries

Suchawadee Saisangtham[1], Chutiwat Likitaporn[2], Pornnapa Kasemsiri[3], Jiaqian Qin[4,5], Manunya Okhawilai[4,5], Pranut Potiyaraj[5,6], Hiroshi Uyama[7]*

[1]Multidisciplinary Program in Petrochemistry and Polymer Science, Faculty of Science, Chulalongkorn University, 10330 Bangkok, Thailand
[2]Nanoscience and Technology Interdisciplinary Program, Graduated School, Chulalongkorn University, 10330 Bangkok, Thailand
[3]Department of Chemical Engineering, Faculty of Engineering, Khon Kaen University, 40002 Khon Kaen, Thailand
[4]Metallurgy and Materials Science Research Institute, Chulalongkorn University, 10330 Bangkok, Thailand
[5]Center of Excellence in Responsive Wearable Materials, Chulalongkorn University, 10330 Bangkok, Thailand
[6]Department of Materials Science, Faculty of Science, Chulalongkorn University, 10330 Bangkok, Thailand
[7]Department of Applied Chemistry, Graduate School of Engineering, Osaka University, 565-0871 Osaka, Japan

Abstract. This research aims to fabricate a polyacrylonitrile (PAN)/bio-based polyurethane (bio-based PU) separator for a Zn-ion battery. PAN/bio-based PU electrospun fiber mats at 75/25 were prepared via electrospinning technique using Taguchi experimental design with three parameters and four levels. It was found that all fiber mats illustrated smooth and continuous fiber. The properties of the electrospun fiber mats were optimized in accordance with the grey relational method. Furthermore, the fiber mats prepared from 14 wt% polymer concentration, 25 kV of applied voltage, and 16 cm of distance from tip to collector were determined to be the most suitable fabrication condition exhibiting an ionic conductivity of 3.11 mS/cm, the tensile strength of 44.16 MPa, and electrolyte uptake of 1,971%. Moreover, the fiber mats showed no dimensional change at a temperature of 150 °C because of the incorporation of bio-based PU in the polymer network. The electrochemical stability of the Zn-ion battery with the developed separator was greater than that of the commercial glass fiber separator. Thus, the PAN/bio-based PU electrospun fiber can be considered a promising candidate as a separator for Zn-ion batteries.

Keywords: polymer blends and alloys, polymer membranes, bio-based polyurethane separator, zinc ion battery

1. Introduction

Energy storage devices are one of the most vital innovations in the development of materials to make a rechargeable battery for high-performing devices. Lithium-ion batteries (LIBs) have been widely applied as commercial energy storage devices, owing to the advantages of high efficiency in terms of delivering energy; however, they came with disadvantages, that is, safety problems and high cost [1]. Serving as

an alternative to LIBs, zinc-ion batteries (ZIBs) are currently used for energy storage systems, owing to their high theoretical capacity, low cost, and being more environment-friendly [2, 3]. Separators play a key role in all batteries, as they allow the flow of ions and, at the same time, prevent electrical contact between the two electrodes of opposite polarity that may cause a short circuit [4]. The separator should have good thermal and dimensional stabilities,

chemical resistance to degradation by electrolyte and reactant products, and good mechanical properties. In particular, the separator should exhibit high porosity and uniform pore size to absorb and retain electrolytes and minimize ionic resistance [5]. Among the various techniques used to produce porous structures, including phase inversion [6, 7] and thermally induced phase separation [8], electrospinning is a simple and versatile technique that uses electrostatic forces to produce polymer fibers that have nano- to micron-size fiber diameter with high porosity [9]. The fibers obtained from this process are found to have a high surface area, are lightweight, and are suitable as a battery separator [10]. Most polymer-based separators used today are based on polypropylene and polyethylene as it is cost-effective and has good strength [11]. However, these separators exhibited low thermal stability, with a melting temperature of around 160 °C [12]. Poly(vinylidene fluoride) (PVDF) [13, 14], poly(vinylidene fluoride-*co*-hexafluoropropylene) (PVDF-HFP) [15], and poly(methyl methacrylate) [16] have been used to develop polymer-based electrolyte and separator. Polyacrylonitrile (PAN) possesses greater thermal stability with a melting point of 320 °C [12]; moreover, it was also reported to effectively suppress dendrite formation due to its high mechanical strength [17]. However, PAN electrospun fiber mat was observed to shrink thermally at only 150 °C and showed poor mechanical strength; this could limit applications where high strength and flexibility are needed, for example, wearable devices [18, 19]. In this context, the polymer blend of PAN with high flexibility polyurethane (PU) has been developed in this research. PU can be synthesized from polyol, diisocyanate, and chain extender of a diol with catalyst. The PU structure can vary by the chemical substance to meet the property requirements. Bio-based PU has been used extensively for the last few decades for its low environmental impact and biodegradability, replacing petroleum-based PU [20]. Among several electrospinning parameters, polymer concentration, applied voltage, and collector-to-needle tip were mostly reported to affect the overall properties of the obtained fiber mats [21, 22]. Therefore, they were chosen as parameters to be studied. Design of experiment (DOE) is generally used to analyze the impact of individual components and their interaction [23, 24]. One of the most effective DOE methods was proposed by Taguchi, wherein the optimum mix proportions of

polymer were designed with a minimum number of experiments [25, 26]. This approach has been used to optimize a single response and to determine the main factors responsible for the response. For the multi-response optimization problem, Taguchi coupled with grey relational analysis is used to optimize the multiple responses by converting them into a single relational grade. PAN/petroleum-based PU polymer gel electrolytes have been fabricated for use in LIBs [27]. However, there is yet no study reporting on the development of PAN/bio-based PU for ZIB separators with relatively different electrolyte conditions and involved electrode reactions to LIBs. Therefore, the objectives of this work are to fabricate ZIB separator from PAN/bio-based PU via the electrospinning technique. The relevant properties of the separator, including morphology, pore size, porosity, tensile strength, electrolyte uptake, and ionic conductivity, are characterized. Moreover, designing the properties of electrospun separator using the experimental design proposed by Taguchi and optimization using grey relational analysis has rarely been examined.

2. Experiment
2.1. Materials
PAN having an average M_w of 150 000 g/mol, dibutyltin dilaurate (95%), and zinc trifluoromethanesulfonate (98%) were purchased from Sigma Aldrich Corporation (Missouri, USA). Polycaprolactone diol having an average M_n of 2000 g/mol, and ethylene glycol (AR Grade) were purchased from Sigma Aldrich Corporation (Missouri, USA). Dimethylformamide was supplied from RCI Labscan limited (Bangkok, Thailand). Partially bio-based diisocyanate (Tolonate™ X FLO 100) was kindly provided by Vencorex Co. Ltd. (Le-Pont-de-Claix, France).

2.2. Synthesis of bio-based PU
In this study, bio-based PU was synthesized using polycaprolactone diol, partially bio-based diisocyanate, and ethylene glycol at a molar ratio of 2.1:1:1 in a four-necked round-bottom flask equipped with a mechanical stirrer, thermometer, and condenser. All reactant was charged in the reactor, having dimethylformamide solvent with an addition of dibutyltin dilaurate catalyst. The reaction was carried out at a temperature of 70 °C under an N_2 atmosphere. Effects of pre-polymerization times before adding ethylene glycol chain extender and total reaction
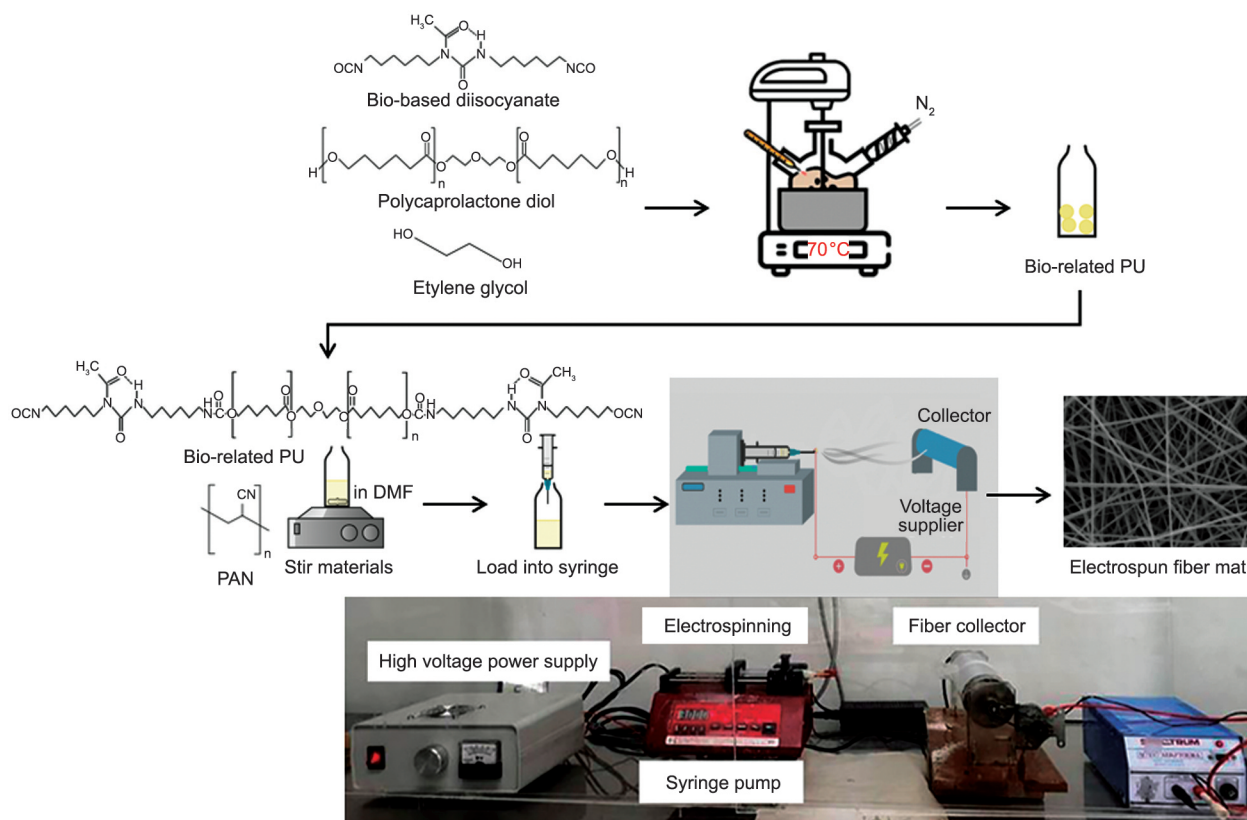
Figure 1. Synthetic route of bio-based PU and electrospinning setup.

times on their M_w and polydisperse index (PDI) were examined. The as-synthesized bio-based PU solution was dropped into a large amount of ethanol and then filtered. The synthetic route of bio-based PU is shown in Figure 1.

2.3. Electrospinning of PAN/bio-based PU
PAN/bio-based PU electrospun fiber mats having different blending weight ratios in the range of 0–75 wt% were prepared by electrospinning technique. The setup is shown in Figure 1. The PAN/bio-based PU was dissolved in dimethylformamide solvent via mechanical stirring overnight until a homogeneous solution was obtained. The suitable blending weight ratio of PAN/bio-based PU was then fabricated into non-woven fiber mats. The homogeneous solution of PAN/bio-based PU was charged into a 5 ml syringe coupled with a needle having an inner diameter of 0.5 mm and placed in a syringe pump with a controlled flow rate of the polymer solution of 1.5 ml/h. Humidity and temperature during the electrospinning experiment are controlled using an environmental chamber to be 40±3% and 23±2 °C, respectively. The electrospun fiber mats were dried for at least 24 h before further use. The effects of polymer concentration which is associated with solution viscosity

as it increases with the increase of the polymer concentration [28], the applied voltage, and the distance from tip to collector on morphology and fiber diameter of the fiber mats were investigated. The spinning ability of the PAN/bio-based PU was studied at spinning conditions of 8–14 wt% polymer concentration, 19–25 kV applied voltage, and 16–22 cm the collector-to-needle-tip distance. The DOE proposed by Taguchi including the three factors and four levels was given in Tables 1 and 2. The upper and lower limits of each factor were designed based on continuous fiber without beads. The pure PAN electrospun fiber mats fabricated using 10 wt% polymer concentration, 23 kV applied voltage, and 16 cm the collector-to-tip distance was used for the comparative study.

2.4. Characterization
The chemical structure of the bio-based PU was investigated using Fourier-transform infrared spectroscopy (FT-IR). A model of Nicolet 6700 (Thermo Fisher Scientific) spectrometer equipped with an attenuated total reflectance accessory was utilized. All samples were scanned at a resolution of 4 cm^{-1} within the spectral range of 4000–650 cm^{-1}. The obtained results were subtracted with the background spectra.

Table 1. Factors and their levels.

Parameter	Level 1	Level 2	Level 3	Level 4
Polymer concentration [wt%]	8	10	12	14
Applied voltage [kV]	19	21	23	25
Distance from needle tip to collector [cm]	16	18	20	22

Table 2. L_{16} (4^3) orthogonal array.

Sample No.	Polymer concentration [wt%]	Applied voltage [kV]	Distance from needle tip to collector [cm]
1	8	19	16
2	8	21	18
3	8	23	20
4	8	25	22
5	10	19	18
6	10	21	16
7	10	23	22
8	10	25	20
9	12	19	20
10	12	21	22
11	12	23	16
12	12	25	18
13	14	19	22
14	14	21	20
15	14	23	18
16	14	25	16

The average molecular weight of as-synthesized bio-based PU was carried out using gel permeation chromatography Alliance Co. Ltd., model Waters e2695 separations modules. The bio-based PU was dissolved in tetrahydrofuran. The solution was then filtered and injected at a flow rate of 1 mm/min for 100 µl at 35 °C.

The morphology of the PAN/bio-based PU electrospun fiber mats was investigated via scanning electron microscope (SEM) (Hitachi SU-4800). The scanning electron microscope was operated at an accelerating voltage of 3.0 kV and an emission current of 10 mA. The surfaces of the samples were sputter-coated with gold before measurement. The average fiber diameter was determined from hundred measurements using Image J.

The porosity of the electrospun fiber mats was measured using the n-butanol uptake test. The samples were then cut into squares of 1.9 cm². The porosity values were calculated according to Equation (1):

$$\text{Porosity [\%]} = \frac{W_w - W_d}{\rho_b V_d} \cdot 100 \qquad (1)$$

where W_d is the dry weight of the PAN/bio-based PU electrospun fiber mats, W_w is the wet weight of the fiber mats after immersing the sample in n-butanol for 2 h, ρ_b is the density of *n*-butanol, and V_d is the volume of the dry mats. The average value was calculated from three measurements.

The electrospun fiber mat samples were cut into a dimension of 2×2 cm². The electrolyte uptake of the electrospun fiber mats was determined using Equation (2):

$$\text{Electrolyte uptake [\%]} = \frac{W_w - W_d}{W_d} \cdot 100 \qquad (2)$$

where W_d and W_w are the weight of the PAN/bio-based PU electrospun fiber mats before and after immersing the sample in the liquid electrolyte for 1 h, respectively. The average value was calculated from three measurements.

The wettability of the fiber mats by an electrolyte was observed with an electrolyte droplet placed on their surfaces and confirmed by an in-house contact angle analyzer. The electrospun fiber mats were dried in a vacuum overnight to remove all moisture. The contact angle measurements were conducted within 5 sec, often placing one drop of electrolyte on the samples. The final contact angles were obtained as the average of three measurements at room temperature.

The tensile properties of the electrospun fiber mats were characterized at room temperature using a universal testing machine (Tinius Hitachi, model 5ST) according to ASTM D882. The samples with a dimension of 10 mm × 60 mm × 0.02 mm (width × length × thickness) were prepared. The test was carried out with a gauge length of 50 mm and a crosshead speed of 50 mm/min. The tensile test results were obtained by averaging the data of seven measurements of each sample. The flexibility of the electrospun fiber mats was carried out by twisting the 15 cm length of the fiber mats around a 5 mm diameter glass rod, following Zainab *et al.* [29]. The appearance of fiber mats after un-twist was observed.

A potentiostat/galvanostat (PSTrace4 Palm Sens) was utilized for investigating the electrochemical properties. The measurements were performed on an applied 10 mV AC potential from 1 MHz to 1 Hz. The Zn/separator/Zn cell was constructed by inserting the

fiber mats between blocking electrodes made of stainless steel. The membrane thickness and the active area were approximately 200–300 μm and 2.834 cm^2, respectively. Transference number measurement was performed using the DC polarization method using chronoamperometry. A polarization voltage of 10 mV was applied across the sample, and the initial maximum current I_0 and steady-state current I_s were recorded. The ionic conductivity could be worked out according to Equation (3). The average value was from three measurements:

$$\text{Ionic conductivity [S/cm]} = \frac{\text{thickness}}{\text{bulk resistance} \cdot \text{area}} \tag{3}$$

The thermal dimensional stability test of the fiber mats was carried out. The circular shape sample having a diameter of 19 mm was heated in an oven at a temperature of 90–150 °C for 1 h each, which was modified from Zainab *et al*. [29]. The dimensional change of the samples was calculated according to Equation (4):

$$\text{Thermal dimension stability [\%]} = \frac{A_i - A_f}{A_i} \cdot 100 \tag{4}$$

where A_i and A_f represent the initial and final surface areas of the samples, respectively. The fiber morphology of the electrospun fiber mats before and after heated was observed by SEM.

The voltage response on the electrochemical compatibility of PAN/bio-based PU fiber mats was investigated and recorded as a function of the cycle at room temperature for long-term zinc charge/discharge cycles through the use of a Neware testing system (Shenzhen Neware CT-4008). The charge-discharge cycles of the CR2032 coin cell with symmetric Zn/separator/Zn cells were carried out at a current density of 1 mA/cm. The CR2032 coin cells were assembled by sandwiching the separators between Zn foil and MnO$_2$ electrode in a liquid electrolyte consisting of 2 M zinc triflate to measure the potential range.

Taguchi method containing three factors and three levels was used to optimize the conditions of the UAE process in terms of single-response and multiple responses. The conditions and their variation levels are shown in Table 2. The signal-to-noise ratio (S/N) was used to evaluate the effect of each parameter level for single-response optimization with the help of ANOVA.

The S/N ratios were classified into three classes, namely, (1) nominal-the-better, (2) smaller-the-better, and (3) larger-the-better, which were applied for optimization [30]. In this study, all responses, including pore size and porosity, were minimized for the 'smaller-the-better class', whereas strength, electrolyte uptake, and ionic conductivity were maximized for the 'larger-the-better class'. S/N ratio was analyzed based on Equations (5) and (6), respectively.

$$(S/N) = -10 \cdot \log\left[\frac{1}{R}\sum_{i=1}^{R} y_i^2\right] \tag{5}$$

$$(S/N) = -10 \cdot \log\left[\frac{1}{R}\sum_{i=1}^{R} \frac{1}{y_i^2}\right] \tag{6}$$

where R is the number of all data points, and y_i is the value of ith data point.

To convert multiple responses to single-response optimization via S/N ratio calculation, grey relational analysis was employed. The obtained results from the Taguchi method are then calculated to determine the highest overall grey relational, which represents the optimal parametric combination. Before grey relational analysis, data preprocessing is normally required, which is a process of transferring the original sequence to a comparable sequence that is normalized within the range of 0 to 1 [31]. The reference sequence and comparable sequence can be denoted by $x_0(k)$ and $x_i(k)$ for $i = 1, 2, \ldots, m$; $k = 1, 2, \ldots, n$, respectively, where m is the total number of experiments to be considered and n is the total number of observation data. The appropriate equation for the normalization also depends on the type of the quality characteristic. In this work, the smaller-the-better and the larger-the-better quality characteristics were applied for the normalization of all responses that as expressed in Equations (7) and (8), respectively:

$$x_i(k) = \frac{\max y_i(k) - y_i(k)}{\max y_i(k) - \min y_i(k)} \tag{7}$$

$$x_i(k) = \frac{y_i(k) - \min y_i(k)}{\max y_i(k) - \min y_i(k)} \tag{8}$$

where $x_i(k)$ is the value after grey relational generation, $\min y_i(k)$ is the smallest value of $y_i(k)$ for the kth response, and $\max y_i(k)$ is the largest value of $y_i(k)$ for the kth response.

Grey relational coefficient can be calculated using Equation (9):

$$\gamma\left(x_0^*(k), x_i^*(k)\right) = \frac{\Delta_{min} + \zeta\Delta_{max}}{\Delta_{0i}(k) + +\zeta\Delta_{max}},$$
$$0 < \gamma\left(x_0^*(k), x_i^*(k)\right) \leq 1 \tag{9}$$

where $\Delta_{0i}(k) = \left|x_0^*(k) - x_i^*(k)\right|$

$$\Delta_{max} = \overset{max.}{\forall j} \in \overset{max.}{i \forall k} \left|x_0^*(k) - x_i^*(k)\right|$$

$$\Delta_{min} = \overset{min.}{\forall j} \in \overset{min.}{i \forall k} \left|x_0^*(k) - x_i^*(k)\right|$$

and ζ is the distinguishing coefficient $\zeta \in [0,1]$. If all the process parameters have equal weighting, ζ is set to be 0.5. The grey relational grade (γ) is the average of all grey relational coefficients, which can be determined using Equation (10):

$$\gamma\left(x_0^*, x_i^*\right) = \frac{1}{n}\sum_{k=1}^{n}\beta_k\gamma\left(x_0^*(k), x_i^*(k)\right) \tag{10}$$

Finally, the optimal condition of sugarcane wax extraction can be the level corresponding to the highest value of the average grey relational grade of each factor.

3. Results and discussion
3.1. Synthesis of bio-based PU
Effects of pre-polymerization and polymerization time on M_w of bio-based PU were investigated. From Table 3, M_w of bio-based PU with addition of ethylene glycol chain extender was increased with pre-polymerization time, *i.e.*, from 8500 g/mol at pre-polymerization at 0 h to 10 000 g/mol at 4 h of poly-

merization. This can be attributed to the more reaction occurring between a diisocyanate and poly-caprolactone diol before they were linked by the chain extender resulting in the longer PU chain. It was also observed that the PDI, which refers to the variety of polymer chain lengths, was increased with pre-polymerization time, indicating the more random polymerization of the reaction. The result was consistent with that reported by Sánchez-Adsuar *et al.* [32]. Furthermore, the effect of the synthesis time with an addition of chain extender at the 4th hour of polymerization time on M_w and PDI was investigated. As displayed in Table 4, the M_w of bio-based PU was noted to be greater with polymerization time due to the more reaction time of diisocyanate, polyol, and chain extender. The M_w of bio-based PU increased from 7600 g/mol at 4 h of polymerization time to 28 000 g/mol at 100 h of polymerization time. However, the polydispersity index of the bio-based PU was decreased, indicating more homogeneity of the polymer chain. The less increment of M_w with a much longer synthesis time was attributed to the bio-based diisocyanate used in this research having bulk and linear structure, which, in turn, caused low reaction rate between polyol and diisocyanate [32].

The chemical structure of bio-based PU was confirmed by FTIR spectra, as shown in Figure 2. A broad N–H stretching band of the amide group appeared at 3329 cm^{-1}. The absorption peaks around 1721 cm^{-1} were from asymmetric stretching of the amide carbonyl group, whereas the bands at 2930–2860 cm^{-1} were assigned for the C–H stretching of the polyol [33]. It could be observed that no characteristic peak of -N=C=O of diisocyanate was found

Table 3. Molecular weight and dispersity of synthesized bio-based PU with different pre-polymerization times.

Prepolymerization time [h]	Polymerization time [h]	Average molecular weight [g/mol]	Dispersity [–]
0	12	8 500	2.1
2	12	9 200	2.2
4	12	10 000	2.4

Table 4. Molecular weight and dispersity of synthesized bio-based PU with different synthesis times.

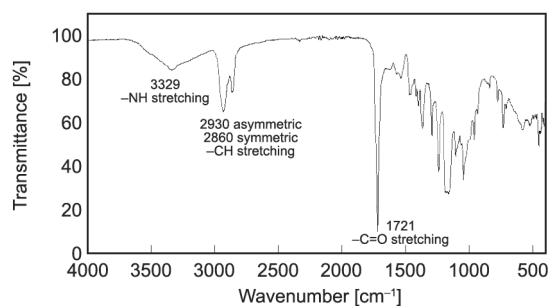| Synthesis time [h]	Prepolymerization time [h]	Average molecular weight [g/mol]	Dispersity [–]
4	4	7 600	2.3
12	4	10 000	2.4
24	4	20 000	2.2
100	4	28 000	2.1

Figure 2. FTIR spectra of as-synthesized bio-based PU.

around 2260 cm^{-1}, indicating that all diisocyanate group was formed into urethane linkage.

3.2. Morphology of the PAN/bio-based PU electrospun fiber mats with different blending ratios

Morphology of PAN/bio-based PU electrospun fiber mats with different blending weight ratios in the range of 0–75 wt% of bio-based PU was characterized. The electrospun was prepared at the same electrospinning conditions, *i.e.*, 10 wt% polymer concentration, 21 kV applied voltage, and 16 cm distance from needle tip to collector. As shown in Figure 3, the pure bio-based PU cannot be spun into fiber as it was observed to be in droplet and melt morphology on the collector, which could be due to the low M_w of bio-based PU resulting in less polymer chain entanglement to produce such continuous fibers [34]. As PAN contents in the blend increased, the fiber was noticed. At 25 wt% of PAN, the fibers with large amounts of beads and some connected points were observed. The increase of PAN content to 50 wt% resulted in continuous fiber but with fewer amounts of beads and some unstable polymer jet. The stable, smooth, and continuous fiber without beads were formed using the PAN/bio-based PU at 75/25. It is consequently used for further studies.

3.3. Fiber diameter and distribution of the PAN/bio-based PU electrospun fiber mats

Following DOE proposed by Taguchi's method in terms of providing continuous length, randomly arranged, not curly, and no appearance of beads, it is necessary to note that the fiber with beads exhibited a negative effect on the properties of the fiber mats [12]. Sixteen experiments were carried out under the conditions shown in Table 2. Figure 4 illustrates the morphology of PAN/bio-based PU electrospun, showing the continuous fiber with no formation

of beads with a diameter ranging from 260 to 1,160 nm.

Influences of processing conditions, *i.e.*, the concentration of polymer solutions, applied voltage, and distance from tip to collector, on fiber diameter of PAN/bio-based PU electrospun fiber mats were investigated according to the Taguchi technique. As seen from Figure 5a, the fiber diameter sharply enlarged with increasing concentration of polymer solution, *i.e.*, from 271 nm at 8 wt% concentration to 1,140 nm at 14 wt% concentration, which can be accounted to be 320% increment. This can be due to the polymer in polymer solution being at a higher concentration. As the polymer solution was ejected from the tip, the solvent evaporated, and the polymer solidified into an enlarged fiber diameter at the collector. It was also attributed to the more viscous, higher surface tension and viscoelastic force of the solution [34]. The result was in accordance with that reported by Jacob *et al*. [35]. The applied electric field is an important parameter in the electrospinning process due to its direct influence on the dynamics of the fluid flow. When a sufficiently high voltage is applied to a droplet, the body of the liquid droplet becomes charged, electrostatic repulsion counteracts the surface tension, and the droplet is stretched at a critical point of liquid stream eruption that is known as the Taylor cone. The fibers then oscillate and stretch, resulting in diameters as small as a nanometer. As shown in Figure 5b, with increasing applied voltage, a smaller fiber diameter was observed.

Distance from needle tip to the collector is the length of time the polymer fibers have flicked and stretched [36]. It should be noted from Figure 5c that as the distance from needle tip to collector increases, a smaller diameter was obtained (*p*-value < 0.005). The smallest fiber was produced at the concentration of 8 wt%, applied voltage of 25 kV, and distance from tip to collector of 22 cm, whereas the largest fiber was from the concentration of 14 wt%, applied voltage of 23 kV, and the distance from tip to collector of 18 cm. The opposite trend of S/N ratio on the experimental result confirmed the accuracy of the result. The commercial glass fiber separator revealed brittle nature with discontinuous fiber. The average diameter of the glass fiber was around 580±150 nm. As per these results, the correlations for predicting fiber diameter of PAN/bio-based PU were developed by multi-linear regression as shown in Table 5.
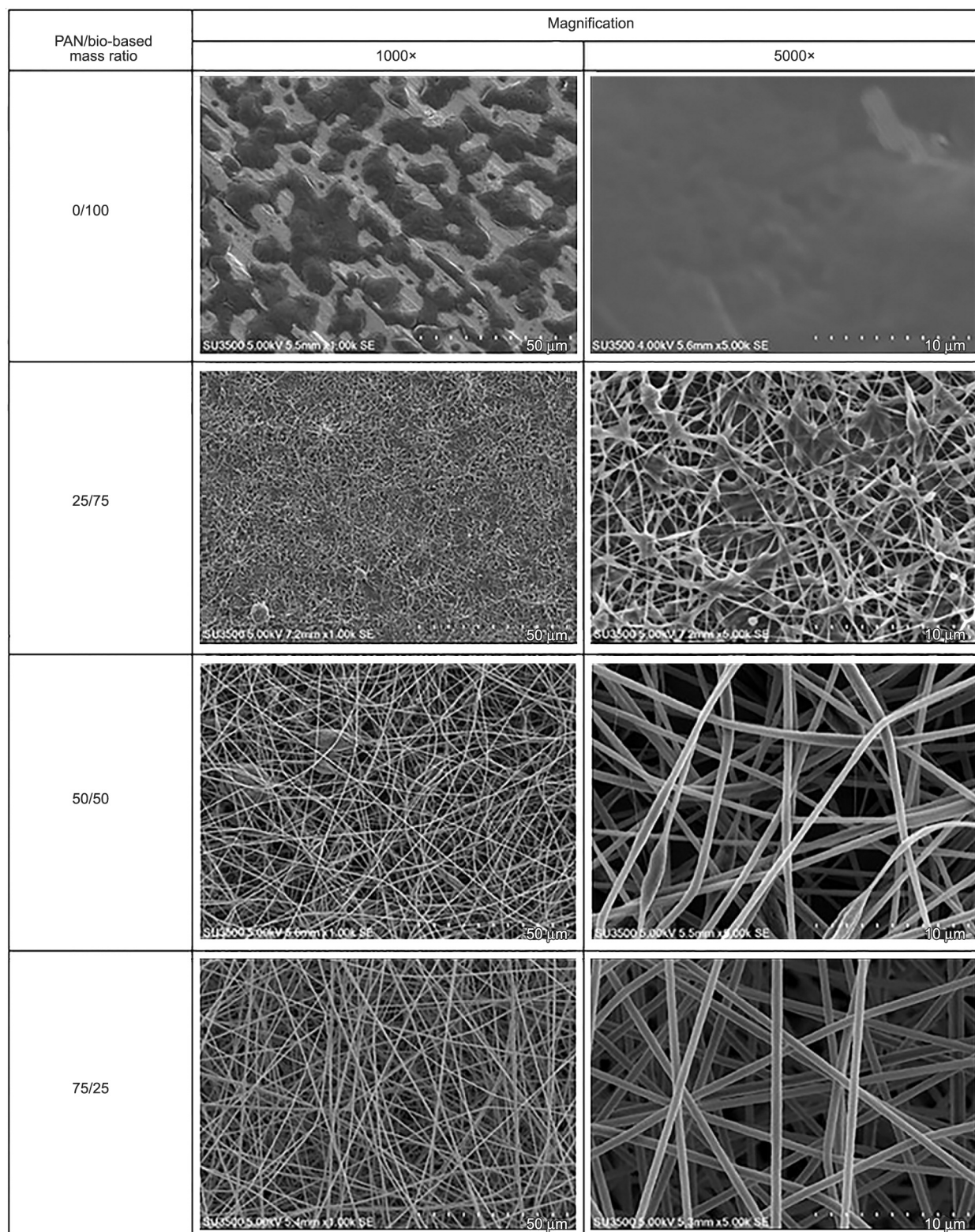
Figure 3. SEM images of PAN/bio-based PU electrospun with various mass ratios ranging from 0 to 75 wt% of PAN.

3.4 Pore size and porosity of PAN/bio-based PU electrospun fiber mats

Separators should have small mean pore sizes and uniform pore size distributions as it can effectively prevent short circuits caused by dendrite growth or the migration of the active material particles between battery electrodes. Uniform pore size distributions can avoid the nonuniform current densities across the electrode-separator interfaces [37]. Figure 6 shows the relationship between pore size and fiber diameter with the concentration of polymer, applied voltage, and distance from tip to collector. As shown in
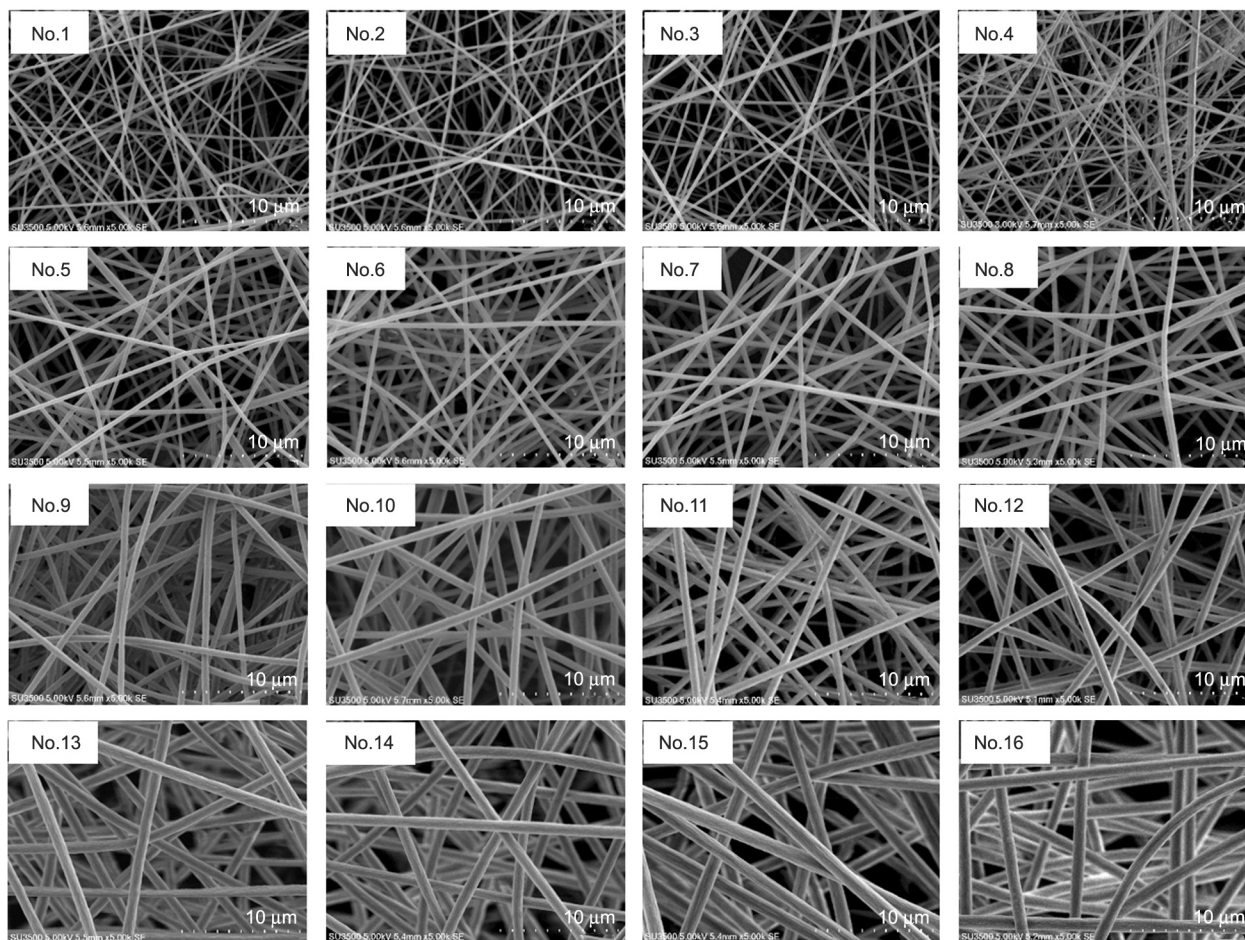
Figure 4. Morphology of PAN/bio-based PU prepared from different conditions regarding Taguchi DOE.

Figure 6a, the average pore size of the PAN/bio-based PU fiber mats increased significantly with increasing polymer concentration, *i.e.*, from 2.15 µm of the 8 wt% concentration to 3.54 µm of the 14 wt% concentration. As can be noted in Figures 6b and 6c, significant decreases in terms of pore size were observed with increasing applied voltage and distance from tip to collector. It should be noted that the pore size of PAN/bio-based PU fiber mats showed a similar trend to fiber diameter. It may be due to the higher concentration of polymer solution that provided a large fiber diameter that resulted in a smaller number of fibers; thus, a larger pore size was obtained. In contrast, the small fiber diameter of fiber mats exhibited many numbers of fiber thus, smaller pore sizes were noticed; in the same way, similar relation has been reported by Lowery *et al*. [38] in their work for electrospun poly(3-caprolactone) fibrous mats.
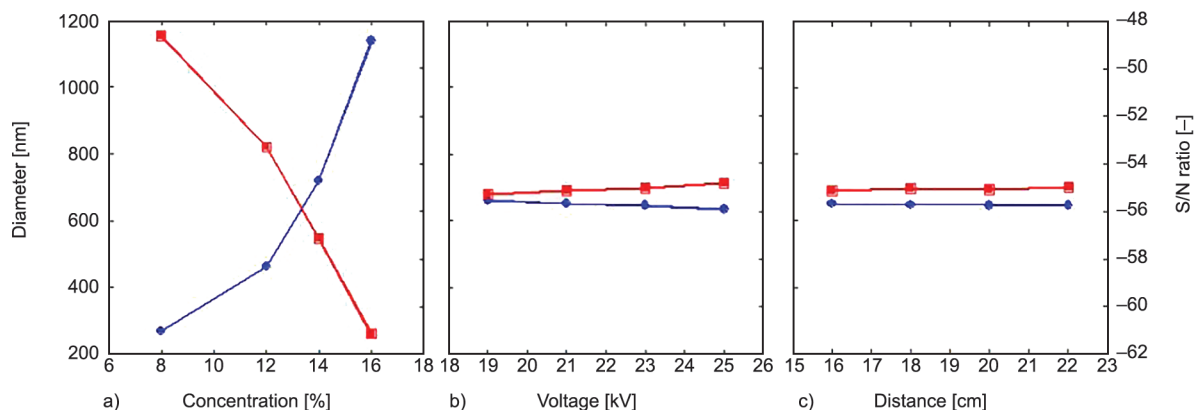

Figure 5. Effect of (a) concentration, (b) applied voltage, and (c) distance from tip to collector on (●) fiber diameter and (■) S/N ratio of PAN/bio-based PU at 75/25.

Table 5. Predicting properties of PAN/bio-based PU by multi-linear regression.

Properties	Predicting equation
Fiber diameter [nm]	$-821.85 + 143.35X_1 - 4.08X_2 - 0.87X_3$
Pore size [μm]	$-0.015 + 0.598X_1 + 0.226X_2 - 0.005X_3$
Porosity [%]	$106.378 + 0.846X_1 - 0.364X_2 - 0.591X_3$
Electrolyte uptake [%]	$1742.12 + 34.613X_1 - 2.691X_2 - 11.156X_3$
Tensile strength [MPa]	$-6.3226 + 2.965X_1 + 0.336X_2 + 0.1348X_3$
Ionic conductivity [S/cm]	$4.3891 + 0.1909X_1 - 0.1060X_2 - 0.0995X_3$

Note: X_1, X_2, X_3 are the concentration of polymer [wt%], applied voltage [kV], and distance from tip to collector [cm].

The smallest pore size of 2.02 μm was produced at the concentration of 8 wt%, applied voltage of 25 kV, and distance from tip to collector of 22 cm. Meanwhile, the largest pore size of 3.70 μm was at the concentration of 14 wt%, applied voltage of 23 kV, and distance from tip to collector of 18 cm. The pore size of the commercial glass fiber separator cannot be measured correctly due to its non-uniformity structure. Table 6 exhibits the results from ANOVA analysis, indicating that the concentration of polymer was the main factor affecting the pore size of the electrospun fiber mats, calculated to be 99.45% contribution. From the result, the correlations for predicting pore size of PAN/bio-based PU were developed by multi-linear regression, as shown in Table 5. The porosity of the sample has been determined as one crucial parameter affecting the efficiency of the separator. The porosity values of PAN/bio-based PU electrospun fiber mats were in the range of 93.30–98.65%. It should be noted from Figure 7

Table 6. ANOVA analysis results

Properties		Factor		
		Polymer concentration	Applied voltage	Distance from tip to collector
Pore size				
v^{**}	[–]	1.498	0.001	0.007
Contribution	[%]	99.452	0.053	0.495
Porosity				
v^{**}	[–]	21.464	3.945	10.335
Contribution	[%]	60.049	11.037	28.914
Electrolyte uptake				
v^{**}	[–]	32 732.708	246.824	3381.175
Contribution	[%]	90.022	0.679	9.299
Tensile strength				
v^{**}		269.21	3.25	0.51
Contribution	[%]	98.62	1.19	0.19
Ionic conductivity				
v^{**}	[–]	1.049	0.302	0.283
Contribution	[%]	64.177	18.480	17.383

Remark: Degree of freedom = 3

that the porosity of the samples exhibited a similar trend to pore size, *i.e.*, the porosity of the sample increased with increasing pore size. The result was in accordance with that reported by Ohzawa *et al.* [39]. Moreover, the porosity of the commercial glass fiber separator was measured to be 91.34%. It is clearly seen that the porosity of the PAN/bio-based PU fiber mats was greater than that of a commercial separator. In comparison, our porosity value was higher than those reported in the system of poly(vinylidene fluoride)/cellulose acetate/$AgTiO_2$ nanofibers polymer electrolyte, having the porosity value in the range of 86 and 88% [40]. Table 6 exhibits the results from ANOVA analysis
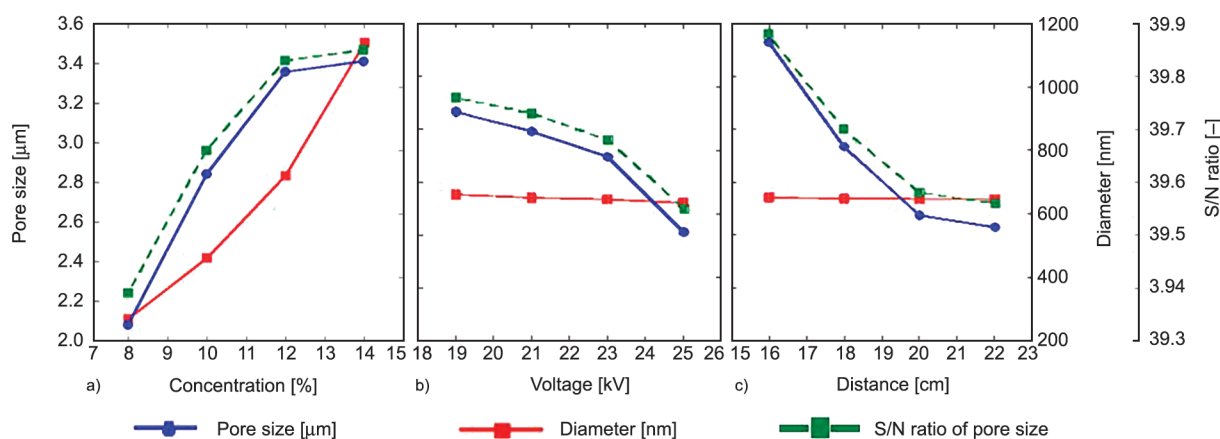

Figure 6. Effect of (a) concentration, (b) applied voltage, and (c) distance from tip to collector on (●) pore size, (■) diameter and (■) S/N ratio of PAN/bio-based PU at 75/25.
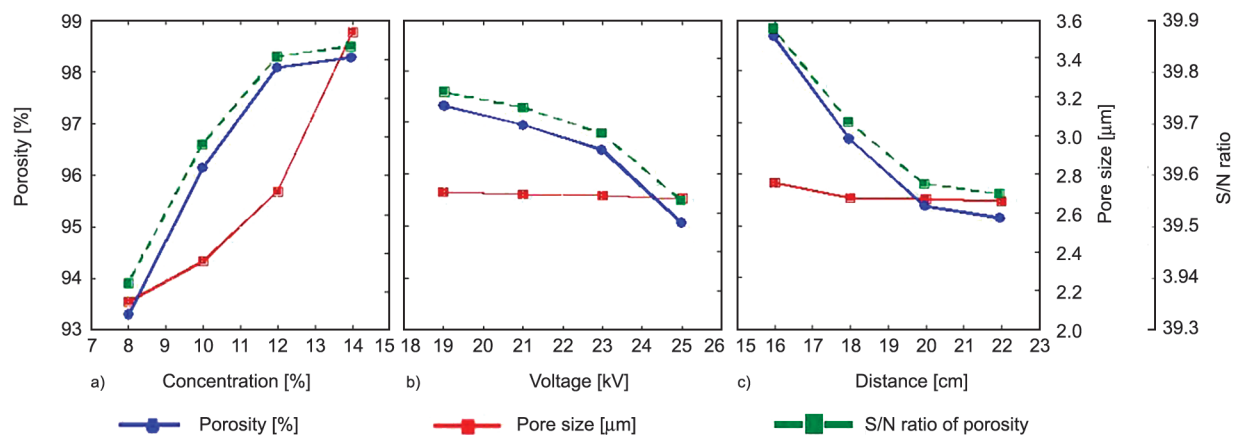
Figure 7. Effect of (a) concentration, (b) applied voltage, and (c) distance from tip to collector on (●) porosity, (■) pore size and (■) S/N ratio of PAN/bio-based PU at 75/25.

Table 7. Average values of relevant properties for PAN/bio-based PU electrospun fiber mats.

Sample No.	Fiber diameter [nm]	Pore size [μm]	Porosity [%]	Electrolyte uptake [%]	Tensile strength [MPa]	Ionic conductivity [S/cm]	Contact angle [°]
1	277±62	2.44±1.00	99.03±0.47	1800.0±7.3	20.92±1.76	2.07±0.25	68.2±0.25
2	263±43	2.12±0.75	96.09±0.23	1789.5±7.5	25.14±3.45	2.10±0.27	69.1±0.35
3	279±51	2.03±0.59	90.71±0.26	1700.0±6.7	26.68±1.71	1.12±0.19	64.7±0.42
4	262±69	2.02±0.66	87.36±0.52	1650.0±3.5	25.60±2.43	1.08±0.26	81.7±0.73
5	483±83	2.26±0.73	94.25±0.17	1820.0±2.4	34.90±2.68	2.86±0.31	71.0±0.72
6	478±69	2.35±0.74	97.09±0.25	1840.0±4.3	37.78±2.14	2.39±0.27	70.2±0.81
7	446±56	2.38±0.74	96.60±0.98	1835.0±1.5	36.57±1.45	2.18±0.31	75.8±0.27
8	441±48	2.45±0.76	96.69±0.35	1834.3±4.3	37.45±1.24	1.67±0.25	81.7±1.32
9	755±42	2.74±0.86	98.36±0.24	1878.3±4.9	40.90±0.83	2.54±0.17	68.9±1.21
10	749±45	2.85±1.22	98.95±0.39	1868.1±3.6	40.76±1.23	2.09±0.16	81.7±0.38
11	695±50	2.65±0.92	98.66±0.51	1927.8±6.2	40.28±0.35	2.92±0.37	88.2±0.32
12	683±51	2.64±1.11	96.38±0.19	1905.0±7.9	41.00±1.37	1.93±0.45	86.5±0.48
13	1127±50	3.39±1.83	97.67±0.25	1930.0±1.9	43.37±0.42	2.78±0.28	89.5±0.38
14	1113±63	3.47±1.32	95.71±0.15	1927.8±6.1	40.89±0.57	3.06±0.21	87.0±0.19
15	1163±44	3.70±1.73	99.97±0.37	1950.0±6.4	43.59±0.43	2.38±0.25	87.9±1.36
16	1155±57	3.59±1.73	99.82±0.85	1971.4±5.1	44.16±1.25	3.11±0.16	78.5±1.73

indicating that the concentration of polymer was the main factor affecting the pore size of the electrospun fiber mats, calculated to be 60.05%. From the result, the correlations for predicting pore size of PAN/bio-based PU were developed by multi-linear regression, as shown in Table 5. Table 7 summarizes the pore size and porosity values of all 16 samples.

3.5. Electrolytes uptake of PAN/bio-based PU electrospun fiber mats

A separator should be able to absorb and retain electrolytes. Electrolyte uptake is needed for ion transport. Large liquid electrolyte uptake is essential for separators because the amount of liquid electrolyte between electrodes can affect the internal ionic resistance of the cell [41]. The electrolyte uptake of

PAN/bio-based PU electrospun fiber mats was in the range of 1,650 to 1,971%, which is greater than 948% of the commercial glass fiber separator. The electrolyte uptake relates to the porosity of the membrane. Consequently, the discussion of electrolyte uptake is made in relation to porosity. Figure 8 show the relationship between electrolyte uptake and porosity with concentration, applied voltage, and distance from tip to collector. It can be observed that the electrolyte uptake of the samples increased with increasing porosity and vice versa. The result was consistent with Ma *et al.* [12]. It was found that the membrane with maximum porosity of 61±2.5% showed an electrolyte uptake of 363±15%. Liu *et al.* [42] reported that the PVDF/thermoplastic PU/PAN fiber mats have electrolyte uptake in the range of 227–331%, depending on the porosity value (45–88%). It was
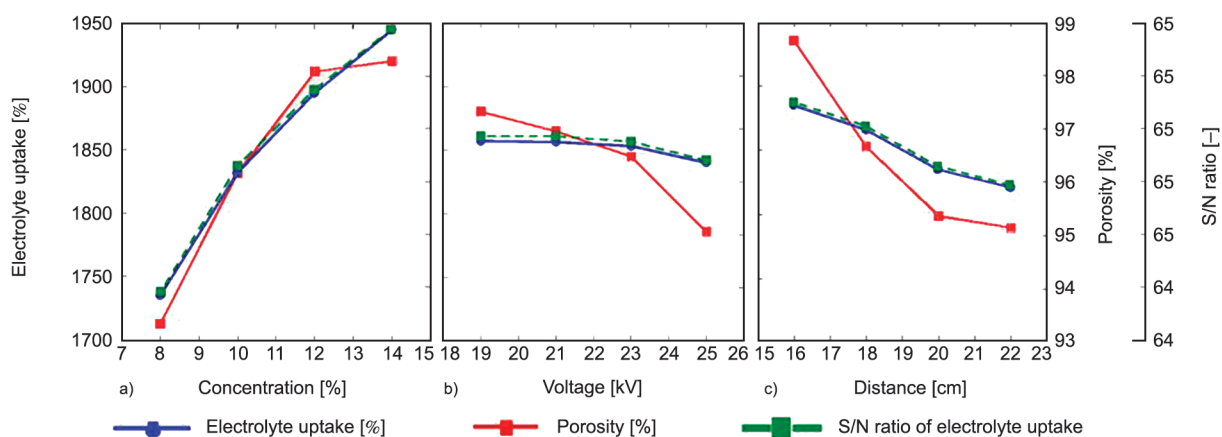
Figure 8. Effect of (a) concentration, (b) applied voltage, and (c) distance from tip to collector on (●) electrolyte uptake, (■) porosity and (■) S/N ratio of PAN/bio-based PU at 75/25.

found that our membrane provided much greater electrolyte uptake, which might be due to the higher porosity and hydrophilic nature of the PAN/bio-based PU than the pure PAN and the PVDF/thermoplastic PU/PAN fiber mats containing PVDF as it is highly hydrophobic to the aqueous-based electrolyte. Table 6 exhibits the results from ANOVA analysis, indicating that the concentration of polymer was the main factor affecting the pore size of the electrospun fiber mats, calculated to be 90.02%. From the result, the correlations for predicting pore size of PAN/bio-based PU were developed via multi-linear regression, as shown in Table 5.

3.6. Tensile properties of PAN/bio-based PU electrospun fiber mats

A separator must be sufficiently strong and must not constrict in order to fulfill mechanical requirements during the battery assembling process [42].

The tensile strength of PAN/bio-based PU electrospun fiber mats was in the range of 20 to 44 MPa. Figure 9 show the relationship between tensile strength and fiber diameter with concentration, applied voltage, and distance from tip to collector. It is noticed in Figure 9a that the tensile strength of the samples showed a similar trend to fiber diameter, *i.e.*, as the fiber diameter increased, the tensile strength increased. Xu *et al.* [43] reported the results of high tensile strength of polyimide and poly(m-phenylene isophthalamide) separator having the value of 34.3 MPa. Interestingly, our separator from PAN/bio-based PU electrospun fiber mats showed the highest tensile strength of 44 MPa. Accordingly, a minimum separator's tensile strength of 13 MPa is required for most winding processes in cylindrical battery manufacturing [44]. The tensile strength of our PAN/bio-based PU electrospun fiber mats was higher than the minimum requirement for the separator. From the
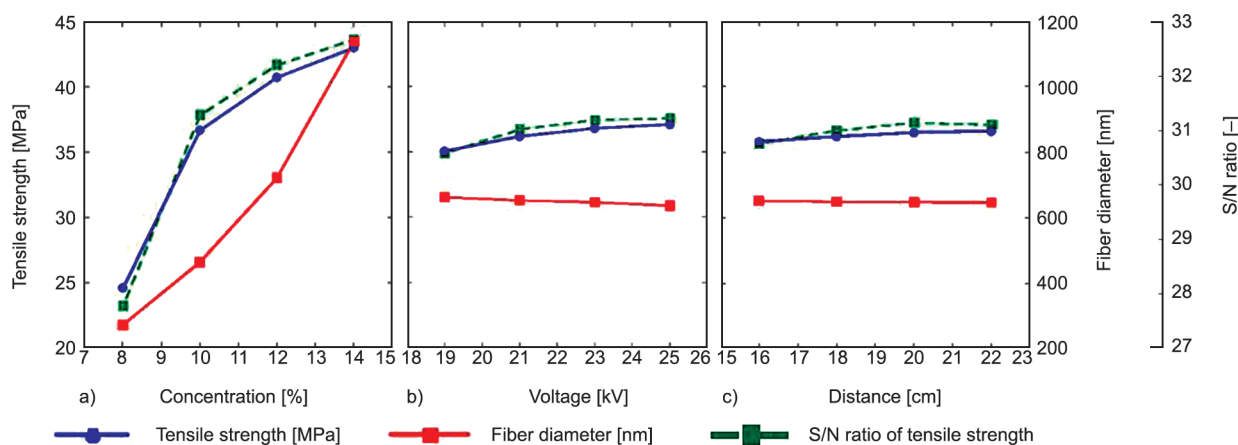

Figure 9. Effect of (a) concentration, (b) applied voltage, and (c) distance from tip to collector on (●) tensile strength (■) fiber diameter and (■) S/N ratio of PAN/bio-based PU electrospun fiber mats.

Figure 10. Flexibility test of PAN/bio-based PU electrospun fiber mats.

result, the correlations for predicting tensile strength of PAN/ bio-based PU were developed via multi-linear regression, as shown in Table 5. Table 6 exhibits the results from ANOVA analysis, indicating that the concentration of polymer was the main factor affecting the pore size of the electrospun fiber mats, calculated to be 98.62%.

Figure 10 presents the twisting behavior of PAN/bio-based PU electrospun fiber mats by flexibility test. The fiber mats possessed excellent flexibility and considerable mechanical strength, did not mechanically crack and can be twisted several times without breaking. Therefore, fiber mats can be a promising material for flexible batteries.

3.7. Ionic conductivity of PAN/bio-based PU electrospun fiber mats

Ionic conductivity has much significance in terms of characterizing a battery separator. It determines battery capacity, rate performance, fast charge capability, overall cell resistance, and cycle life [43]. The Nyquist plot has been used to explain insight into the possible phenomena or mechanism of ion transport in an equivalent circuit model system [44]. The ionic conductivity of the electrolyte-immersed separator

was determined from the bulk resistance value, *i.e.*, the *x*-intercept of extrapolated Nyquist plot at the high-frequency end of real *Z*. A separator with high porosity is generally characterized by sufficient ionic conductivity of a battery cell. The ionic conductivity of PAN/bio-based PU electrospun fiber mats was in the range of 1.08 to 3.11 mS/cm. Figure 11 show the relationship between ionic conductivity and porosity with concentration, applied voltage, and distance from tip to collector. It is observed that the ionic conductivity has a similar trend to the porosity of the electrospun fiber mats, *i.e.*, the ionic conductivity increased with porosity and vice versa. Higher porosity would enhance both electrolyte uptake rate as well as ionic conductivity; as a result, higher and faster ionic conductivity may be achieved, thus improving the overall performance of the separator membrane [45, 46]. The result was consistent with that reported by Costa *et al.* [47], who developed a separator from mesoporous PVDF-HFP. Their results indicated that the ionic conductivity increased with increasing porosity value, which is related to high electrolyte uptake. In comparison, the ionic conductivities of the PAN/bio-based PU fiber mats were mostly higher compared to that of the commercial glass fiber separator in ZIBs, having a value of 1.25 mS/cm, Celgard having a value of 0.1 mS/cm, and Whatman filter paper having the value of 0.75 mS/cm [48]. In addition, the improvement of ionic conductivities was related to some polar functional groups in the PAN/bio-based PU fiber mats and conceptual theory review by Aziz *et al.* [49] for the model of ion transport.

From the result, the correlations for predicting ionic conductivity of PAN/bio-based PU were developed by multi-linear regression, as shown in Table 5. From
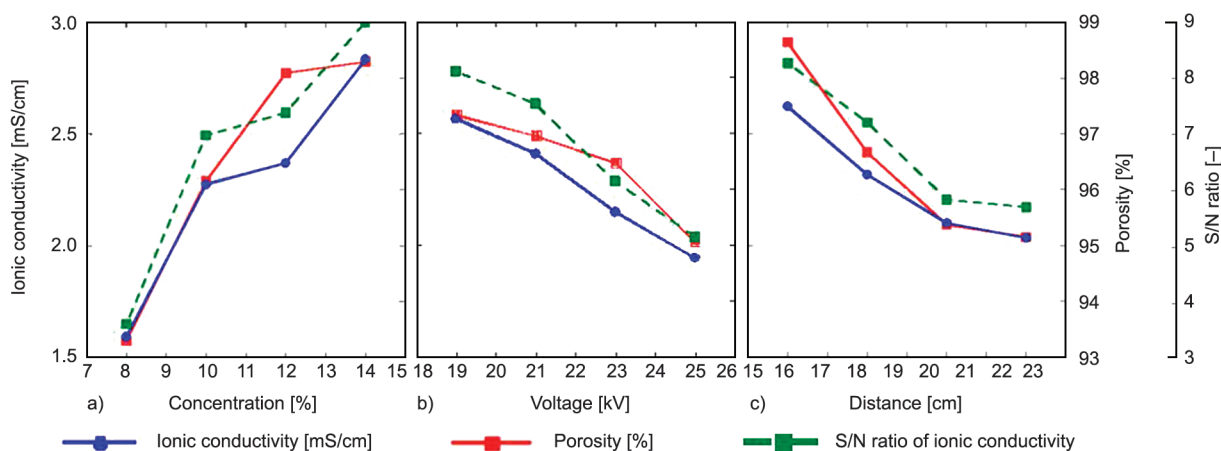

Figure 11. Effect of (a) concentration, (b) applied voltage, and (c) distance from tip to collector on (●) ionic conductivity, (■) porosity and (■) S/N ratio of PAN/bio-based PU at 75/25.

Table 6, the concentration of polymer was the main factor affecting the pore size of the electrospun fiber mats calculated to be 64.18%.

3.8. Contact angle of PAN/bio-based PU electrospun fiber mats

The contact angle of the separator indicates its wettability and ability to absorb electrolytes. Good wettability helps decrease the internal ionic resistance in the battery cell as well as retains electrolytes during cell assembly, and prolongs battery life under normal operation [36]. The contact angle measurements for the PAN/bio-based PU electrospun fiber mats are shown Table 7, indicating no significant effect of the electrospinning parameters. As can be seen, the electrospun fiber mats were hydrophilic in nature and had a static contact angle in the range of 64.7–89.5°, which was less than 90°, whereas the neat PAN electrospun fiber mat showed a hydrophobic nature having the value of 116°, higher than 90°. The result indicated that the addition of bio-based PU could enhance the hydrophilicity of the PAN/bio-based PU electrospun fiber mats, supporting high electrolyte uptake of the fiber mats, as the electrolyte used in this research was an aqueous-based electrolyte and thus greater ionic conductivity.

3.9. Thermal stability of PAN/bio-based PU electrospun fiber mats

Thermal stabilities of the PAN/bio-based PU electrospun fiber mats were observed before and after being heated at a temperature of 150 °C. The morphology of the fiber mats is shown in Figure 12. It can be noted that the fiber mats did not shrink or dimensionally change. From SEM micrograph of the fiber mats with different polymer concentrations, it can be seen that the morphology of the fiber mats at low concentration was curled with no closed pore or melt structure, whereas the fiber mats exhibited more stability against the heat as the morphology was the same to the sample before heating. Therefore, the fiber mats at high concentration had higher thermal stability than the fiber mats at low concentration conditions, indicating that the sample can withstand the heat under battery operation up to 150 °C. It should be noted that even low thermal stability of the electrospun fiber mat with a lower concentration of polymer, the sample can withstand the heat as well, observing from the porous structure and non-close pores.

The dimensional change or shrinkage of the samples can result in an electrical short circuit or thermal runaway, which is extremely concerning because typical thermoplastic materials limit the thermal stabilities of the battery separator [50]. In comparison, the neat PAN electrospun fiber was reported to thermally shrink at 150 °C [19]. The result indicated that with the incorporation of bio-based PU, the thermal dimensional stability of PAN/bio-based PU could be enhanced.

3.10. Optimum procession condition of PAN/bio-based PU electrospun fiber mats using grey relationship analysis

The properties of PAN/bio-based PU fiber mats, including pore size, porosity, electrolyte uptake, tensile strength, and ionic conductivity, were determined to be significant to ideally design the best properties of the separator. The optimization using grey relational analysis is a suitable approach for solving problems with complicated interrelationships between multiple factors and variables. The multiple-response optimization problems can be converted to a single-response optimization. The results of the grey relational analysis are calculated and summarized in Table 8. The grey relational grade represents the degree of similarity between the reference and the comparability sequences. The larger value implies a high degree of similarity with the reference sequence [51, 52]. Consequently, the highest grey relational grade value was obtained with sample No. 16 with the processing condition of 14 wt% concentration of polymer, 25 kV applied voltage, and 16 cm distance from tip to collector, as displayed in Table 9.

The confirmation test was conducted to determine the accuracy of the optimal combination. The predicted grey relational grade ($\hat{\gamma}$) of the PAN/bio-based PU electrospun fiber mats can be calculated as shown in Equation (11):

$$\hat{\gamma} = \gamma_m + \sum_{i=1}^{q}(\gamma_i - \gamma_m) \tag{11}$$

where γ_m is the total mean of grey relational grade, γ_i is the mean of grey relational grade at the optimal level, and q is the number of matching parameters that significantly affected multiple performance characteristics. It was found that the experiment value of 0.8655 was consistent with the predicted value of 0.8297.
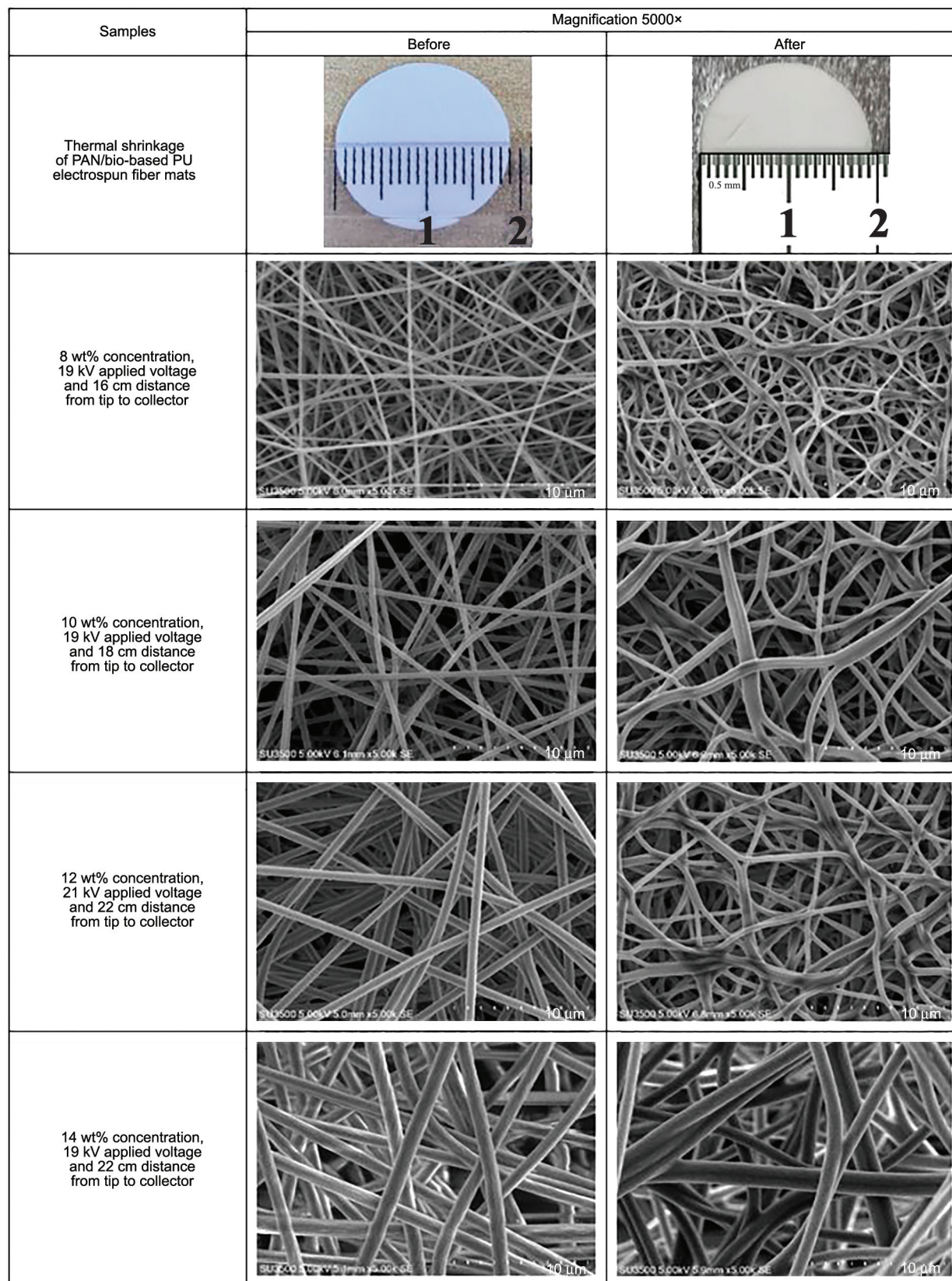
Samples	Magnification 5000×	
	Before	After
Thermal shrinkage of PAN/bio-based PU electrospun fiber mats		
8 wt% concentration, 19 kV applied voltage and 16 cm distance from tip to collector		
10 wt% concentration, 19 kV applied voltage and 18 cm distance from tip to collector		
12 wt% concentration, 21 kV applied voltage and 22 cm distance from tip to collector		
14 wt% concentration, 19 kV applied voltage and 22 cm distance from tip to collector		

Figure 12. Morphology of PAN/bio-based PU electrospun fiber mats before heating and after being heated at 150 °C for 1 h.

Comparably, the PAN/bio-based PU electrospun fiber fabricated using processing condition No. 16 provided the overall properties to be greater than those of electrospun fiber mats.

Table 8. Calculated Grey relational coefficient and Grey relational grade for 16 comparability sequences.

Experiment no.	Grey relational coefficient [–]					Grey relational grade [–]
	Pore size	Porosity	Electrolyte uptake	Tensile strength	Ionic conductivity	
1	0.398	0.870	0.483	0.333	0.377	0.571
2	0.346	0.619	0.469	0.379	0.344	0.526
3	0.334	0.333	0.372	0.399	0.333	0.456
4	0.333	0.405	0.333	0.385	0.340	0.466
5	0.368	0.525	0.515	0.556	0.530	0.527
6	0.382	0.686	0.550	0.646	0.461	0.567
7	0.388	0.652	0.541	0.605	0.391	0.548
8	0.401	0.658	0.540	0.633	0.358	0.551
9	0.466	0.796	0.633	0.781	0.558	0.619
10	0.496	0.861	0.609	0.774	0.435	0.609
11	0.444	0.828	0.786	0.750	0.492	0.635
12	0.441	0.637	0.707	0.786	0.434	0.587
13	0.731	0.733	0.795	0.936	0.786	0.720
14	0.786	0.597	0.786	0.780	0.781	0.680
15	1	1	0.882	0.953	0.733	0.817
16	0.881	0.976	1	1	1	0.866

Table 9. The values of grey relational.

Levels	Polymer concentration	Applied voltage	Distance from tip to collector
1	0.50484	0.60961	0.65976
2	0.54828	0.59531	0.61429
3	0.61249	0.61391	0.57627
4	0.77068	0.61747	0.58596

3.11. Electrochemical stability of the PAN/bio-based PU

The cyclic voltammograms of the batteries with glass fiber and PAN/bio-based PU fabricated at 14 wt% concentration, 25 kV voltage, and 16 cm distance from tip to collector is shown in Figure 13a. The peak of the cell having PAN/bio-based PU electrospun fiber mats located at 1.26 V corresponded to the electron reduction, while another peak located at 1.65 V is attributed to the reverse oxidation process. It was evident that the PAN/bio-based PU had substantially higher electrochemical stability than the commercial glass fiber separator suggesting that the PAN/bio-based PU would be more suitable for Zn ion battery by having higher electrochemical stability in a wider potential range than the commercial separator. The result of cycle life stability of the sample is illustrated in Figure 13b, indicating greater
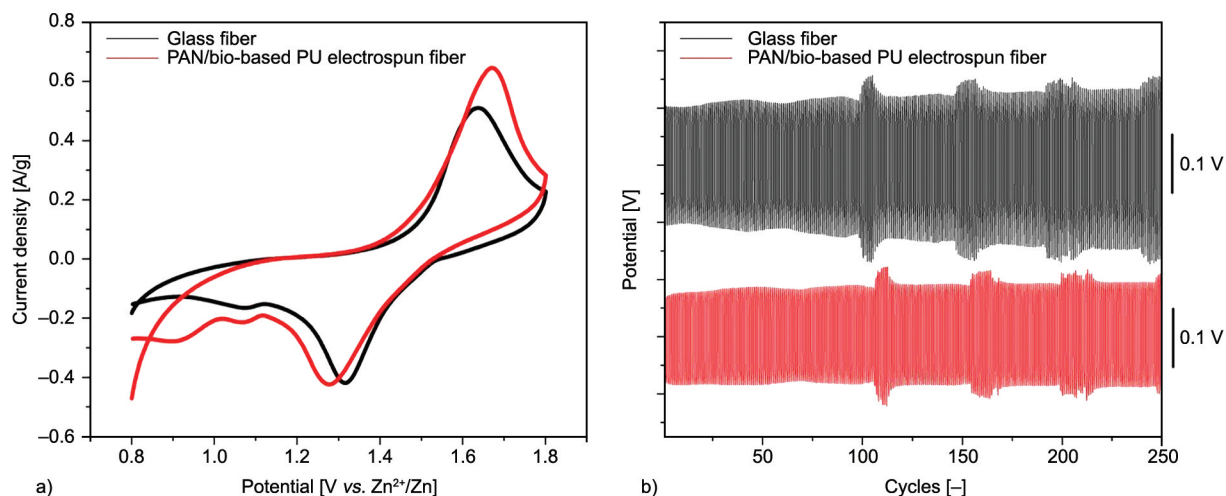
Figure 13. a) CV plots, and b) charge-discharge profile of PAN/bio-based PU electrospun fiber mats compared to commercial glass fiber separator.

charge-discharge stability up to 250 cycles compared to the commercial glass fiber separator.

4. Conclusions

The bio-based PU was prepared using partially bio-based diisocyanate, polycaprolactone diol, and ethylene glycol at a mole ratio of 2.1:1:1, which yields a maximum molecular weight of 28 000 g/mol. PAN/bio-based PU electrospun fiber mats at 75:25 by weight were prepared using the electrospinning technique coupled with Taguchi's design of experiment and grey relational analysis. Among other processing parameters, the concentration of polymer was noted to have significantly affected the properties of the fiber mats. With increasing polymer concentration, fiber diameter increased as well, along with pore size and tensile strength, whereas the increase in porosity resulted in the increase of electrolyte uptake and ionic conductivity. The fiber mats exhibited high flexibility as well. As per the results of optimization using grey relational analysis, the PAN/bio-based PU prepared with the processing condition of 14 wt% polymer concentration, 25 kV of applied voltage, and 16 cm of distance from tip to collector was the most suitable fabrication condition providing all best properties. Moreover, the fiber mats show no dimension and significant morphology changes upon heating to a temperature of 150 °C. The electrochemical stability of the Zn-ion battery with the developed separator was greater than that of the commercial glass fiber separator. It can be concluded that the PAN/bio-based PU electrospun fiber mats are a promising candidate for high flexibility and high-performance separator in Zn-ion batteries.

Acknowledgements

References

[1] Xu W., Wang Y.: Recent progress on zinc-ion rechargeable batteries. Nano-Micro Letters, **11**, 90 (2019).
https://doi.org/10.1007/s40820-019-0322-9

[2] Cao J., Zhang D., Zhang X., Sawangphruk M., Qin J., Liu R.: A universal and facile approach to suppress dendrite formation for a Zn and Li metal anode. Journal of Materials Chemistry A, **8**, 9331–9344 (2020).
https://doi.org/10.1039/D0TA02486D

[3] Wu L., Zhang Y., Shang P., Dong Y., Wu Z-S.: Redistributing Zn ion flux by bifunctional graphitic carbon nitride nanosheets for dendrite-free zinc metal anodes. Journal of Materials Chemistry A, **9**, 27408–27414 (2021).
https://doi.org/10.1039/D1TA08697A

[4] Arora P., Zhang Z.: Battery separators. Chemical Reviews, **104**, 4419-4462 (2004).
https://doi.org/10.1021/cr020738u

[5] Deng C., Jiang Y., Fan Z., Zhao S., Ouyang D., Tan J., Zhang P., Ding Y.: Sepiolite-based separator for advanced Li-ion batteries. Applied Surface Science, **484**, 446–452 (2019).
https://doi.org/10.1016/j.apsusc.2019.04.141

[6] Qi X., Zhang Z., Tu C., Zhu C., Wei J., Yang Z.: Covalent grafting interface engineering to prepare highly efficient and stable polypropylene/mesoporous SiO_2 separator for Li-ion batteries. Applied Surface Science, **541**, 148405 (2021).
https://doi.org/10.1016/j.apsusc.2020.148405

[7] Paul M., Jons S. D.: Chemistry and fabrication of polymeric nanofiltration membranes: A review. Polymer, **103**, 417–456 (2016).
https://doi.org/10.1016/j.polymer.2016.07.085

[8] Tang Y., Lin Y., Ma W., Wang X.: A review on microporous polyvinylidene fluoride membranes fabricated via thermally induced phase separation for MF/UF application. Journal of Membrane Science, **639**, 119759 (2021).
https://doi.org/10.1016/j.memsci.2021.119759

[9] Okhawilai M., Rangkupan R., Kanokpanont S., Damrongsakkul S.: Preparation of Thai silk fibroin/gelatin electrospun fiber mats for controlled release applications. International Journal of Biological Macromolecules, **46**, 544–550 (2010).
https://doi.org/10.1016/j.ijbiomac.2010.02.008

[10] Mirjalili M., Zohoori S.: Review for application of electrospinning and electrospun nanofibers technology in textile industry. Journal of Nanostructure in Chemistry, **6**, 207–213 (2016).
https://doi.org/10.1007/s40097-016-0189-y

[11] Mohammadzad M. K., Pircheraghi G., Sharifi H.: Fabrication, characterization, and electrochemical performance of the HDPE/sepiolite nanocomposite as a novel separator for Li-ion batteries. Express Polymer Letters, **15**, 1063–1080 (2021).
https://doi.org/10.3144/expresspolymlett.2021.86

[12] Ma X., Kolla P., Yang R., Wang Z., Zhao Y., Smirnova A. L., Fong H.: Electrospun polyacrylonitrile nanofibrous membranes with varied fiber diameters and different membrane porosities as lithium-ion battery separators. Electrochimica Acta, **236**, 417–423 (2017).
https://doi.org/10.1016/j.electacta.2017.03.205

[13] de Moraes A. C. M., Hyun W. J., Luu N. S., Lim J-M., Park K-Y., Hersam M. C.: Phase-inversion polymer composite separators based on hexagonal boron nitride nanosheets for high-temperature lithium-ion batteries. ACS Applied Materials and Interfaces, **12**, 8107–8114 (2020).
https://doi.org/10.1021/acsami.9b18134

[14] Li H., Niu D-H., Zhou H., Chao C-Y., Wu L-J., Han P-L.: Preparation and characterization of PVDF separators for lithium ion cells using hydroxyl-terminated polybutadiene grafted methoxyl polyethylene glycol (HTPB-*g*-MPEG) as additive. Applied Surface Science, **440**, 186–192 (2018).
https://doi.org/10.1016/j.apsusc.2018.01.149

[15] Janakiraman S., Agrawal A., Biswal R., Venimadhav A.: An amorphous polyvinylidene fluoride-*co*-hexafluoropropylene based gel polymer electrolyte for sodium-ion cells. Applied Surface Science Advances, **6**, 100139 (2021).
https://doi.org/10.1016/j.apsadv.2021.100139

[16] Ma T., Cui Z., Wu Y., Qin S., Wang H., Yan F., Han N., Li J.: Preparation of PVDF based blend microporous membranes for lithium ion batteries by thermally induced phase separation: I. Effect of PMMA on the membrane formation process and the properties. Journal of Membrane Science, **444**, 213–222 (2013).
https://doi.org/10.1016/j.memsci.2013.05.028

[17] Shim J., Kim L., Kim H. J., Jeong D., Lee J. H., Lee J-C.: All-solid-state lithium metal battery with solid polymer electrolytes based on polysiloxane crosslinked by modified natural gallic acid. Polymer, **122**, 222–231 (2017).
https://doi.org/10.1016/j.polymer.2017.06.074

[18] Chen D., Wang X., Liang J., Zhang Z., Chen W.: A novel electrospinning polyacrylonitrile separator with dip-coating of zeolite and phenoxy resin for Li-ion batteries. Membranes, **11**, 267 (2021).
https://doi.org/10.3390/membranes11040267

[19] Elia G. A., Ducros J-B., Sotta D., Delhorbe V., Brun A., Marquardt K., Hahn R.: Polyacrylonitrile separator for high-performance aluminum batteries with improved interface stability. ACS Applied Materials and Interfaces, **9**, 38381–38389 (2017).
https://doi.org/10.1021/acsami.7b09378

[20] Tavares L. B., Boas C. V., Schleder G. R., Nacas A. M., Rosa D. S., Santos D. J.: Bio-based polyurethane prepared from kraft lignin and modified castor oil. Express Polymer Letters, **10**, 927–940 (2016).
https://doi.org/10.3144/expresspolymlett.2016.86

[21] Fereshteh Z., Fathi M., Kargozar S., Samadihuchaksaraei A.: Implementing Taguchi method to analyze electrospinning parameters influence on Mg-doped fluorapatite nanoparticles-poly(ε-caprolactone) nanocomposite scaffold (Mg-FA NPs/PCL) properties. Polymers Advanced Technologies, **31**, 3114–3125 (2020).
https://doi.org/10.1002/pat.5036

[22] Abdelhakim H. E., Coupe A., Tuleu C., Edirisinghe M., Craig D. Q. M.: Electrospinning optimization of eudragit E PO with and without chlorpheniramine maleate using a design of experiment approach. Molecular Pharmaceutics, **16**, 2557–2568 (2019).
https://doi.org/10.1021/acs.molpharmaceut.9b00159

[23] Ali R., Mehta P., Monou P. K., Arshad M. S., Panteris E., Rasekh M., Singh N., Qutachi O., Wilson P., Tzetzis D., Chang M-W., Fatouros D. G., Ahmad Z.: Electrospinning/electrospraying coatings for metal microneedles: A design of experiments (DOE) and quality by design (QbD) approach. European Journal of Pharmaceutics and Biopharmaceutics, **156**, 20–39 (2020).
https://doi.org/10.1016/j.ejpb.2020.08.023

[24] O'Connor R. A., Cahill P. A., McGuinness G. B.: Effect of electrospinning parameters on the mechanical and morphological characteristics of small diameter PCL tissue engineered blood vessel scaffolds having distinct micro and nano fibre populations – A DOE approach. Polymer Testing, **96**, 107119 (2021).
https://doi.org/10.1016/j.polymertesting.2021.107119

[25] Nazir A., Khenoussi N., Schacher L., Hussain T., Adolphe D., Hekmati A. H.: Using the Taguchi method to investigate the effect of different parameters on mean diameter and variation in PA-6 nanofibres produced by needleless electrospinning. ASC Advances, **5**, 76892–76897 (2015).
https://doi.org/10.1039/C5RA13649K

[26] Sharma S., Choudhary V.: Parametric study for epoxy loaded PMMA microcapsules using Taguchi and ANOVA methods. Express Polymer Letters, **11**, 1023–1036 (2017).
https://doi.org/10.3144/expresspolymlett.2017.96

[27] Tan L., Deng Y., Cao Q., Jing B., Wang X., Liu Y.: Gel electrolytes based on polyacrylonitrile/thermoplastic polyurethane/polystyrene for lithium-ion batteries. Ionics, **25**, 3673–3682 (2019).
https://doi.org/10.1007/s11581-019-02940-7

[28] Hong Y.: Electrospun fibrous polyurethane scaffolds in tissue engineering. in 'Advances in polyurethane biomaterials' (eds.: Cooper S. L., Guan J.) Woodhead, Cambridge, 543–559 (2016).
https://doi.org/10.1016/B978-0-08-100614-6.00019-6

[29] Zainab G., Wang X., Yu J., Zhai Y., Ahmed Babar A., Xiao K., Ding B.: Electrospun polyacrylonitrile/polyurethane composite nanofibrous separator with electrochemical performance for high power lithium ion batteries. Materials Chemistry and Physics, **182**, 308–314 (2016).
https://doi.org/10.1016/j.matchemphys.2016.07.037

[30] Roy R. K.: A primer on the Taguchi method. Society of Manufacturing Engineers, New York (1990).

[31] Pervez H., Mozumder M. S., Mourad A. H. I.: Optimization of injection molding parameters for HDPE/TiO$_2$ nanocomposites fabrication with multiple performance characteristics using the taguchi method and grey relational analysis. Materials, **9**, 710 (2016).
https://doi.org/10.3390/ma9080710

[32] Sánchez–Adsuar M. S., Papon E., Villenave J. J.: Influence of the synthesis conditions on the properties of thermoplastic polyurethane elastomers. Journal of Applied Polymer Science, **76**, 1590–1595 (2000).
https://doi.org/10.1002/(SICI)1097-4628(20000606)76:10<1590::AID-APP14>3.0.CO;2-2

[33] Parnklang T., Boonyanuwat K., Mora P., Ekgasit S., Rimdusit S.: Form-stable benzoxazine-urethane alloys for thermally reversible light scattering materials. Express Polymer Letters, **13**, 65–83 (2019).
https://doi.org/10.3144/expresspolymlett.2019.7

[34] Mi H-Y., Jing X., Napiwocki B. N., Hagerty B. S., Chen G., Turng L-S.: Biocompatible, degradable thermoplastic polyurethane based on polycaprolactone-*block*-polytetrahydrofuran-*block*-polycaprolactone copolymers for soft tissue engineering. Journal of Materials Chemistry B, **5**, 4137–4151 (2017).
https://doi.org/10.1039/C7TB00419B

[35] Jacobs V., Anandjiwala R. D., Maaza M.: The influence of electrospinning parameters on the structural morphology and diameter of electrospun nanofibers. Journal of Applied Polymer Science, **115**, 3130–3136 (2010).
https://doi.org/10.1002/app.31396

[36] Tipduangta P., Sirithunyalug J.: Fundamental and application of electrospinning technology in pharmaceuticals and cosmetics. Isan Journal of Pharmaceutical Sciences, **13**, 1–15 (2017).
https://doi.org/10.14456/ijps.2017.8

[37] Huang X.: Separator technologies for lithium-ion batteries. Journal of Solid State Electrochemistry, **15**, 649–662 (2011).
https://doi.org/10.1007/s10008-010-1264-9

[38] Lowery J. L., Datta N., Rutledge G. C.: Effect of fiber diameter, pore size and seeding method on growth of human dermal fibroblasts in electrospun poly(ε-caprolactone) fibrous mats. Biomaterials, **31**, 491–504 (2010).
https://doi.org/10.1016/j.biomaterials.2009.09.072

[39] Ohzawa Y., Nomura K., Sugiyama K.: Relation between porosity and pore size or pressure drop of fibrous SiC filter prepared from carbonized cellulose-powder preforms. Materials Science and Engineering: A, **255**, 33–38 (1998).
https://doi.org/10.1016/S0921-5093(98)00773-4

[40] Bhute M. V., Kondawar S. B.: Electrospun poly(vinylidene fluoride)/cellulose acetate/AgTiO$_2$ nanofibers polymer electrolyte membrane for lithium ion battery. Solid State Ionics, **333**, 38–44 (2019).
https://doi.org/10.1016/j.ssi.2019.01.019

[41] Yanilmaz M., Zhang X.: Polymethylmethacrylate/polyacrylonitrile membranes *via* centrifugal spinning as separator in Li-ion batteries. Polymers, **7**, 629–643 (2015).
https://doi.org/10.3390/polym7040629

[42] Liu Y., Peng X., Cao Q., Jing B., Wang X., Deng Y.: Gel polymer electrolyte based on poly(vinylidene fluoride)/thermoplastic polyurethane/polyacrylonitrile by the electrospinning technique. The Journal of Physical Chemistry C, **121**, 19140–19146 (2017).
https://doi.org/10.1021/acs.jpcc.7b03411

[43] Xu J., Yuan L., Liang G., Gu A.: Achieving superiorly high heat-dimensional stability, high strength, and good electrochemical performance for electrospun separators in power lithium-ion battery through building unique condensed structure based on polyimide and poly (m-phenylene isophthalamide). Journal of Applied Polymer Science, **138**, 51233 (2021).
https://doi.org/10.1002/app.51233

[44] Li Y., Li Q., Tan Z.: A review of electrospun nanofiber-based separators for rechargeable lithium-ion batteries. Journal of Power Sources, **443**, 227262 (2019).
https://doi.org/10.1016/j.jpowsour.2019.227262

[45] Choi W., Shin H-C., Kim J. M., Choi J-Y., Yoon W-S.: Modeling and applications of electrochemical impedance spectroscopy (EIS) for lithium-ion batteries. Journal of Electrochemical Science and Technology, **11**, 1–13 (2020).
https://doi.org/10.33961/jecst.2019.00528

[46] Liu X., Song K., Lu C., Huang Y., Duan X., Li S., Ding Y. H.: Electrospun PU@GO separators for advanced lithium ion batteries. Journal of Membrane Science, **555**, 1–6 (2018).
https://doi.org/10.1016/j.memsci.2018.03.027

[47] Costa C. M., Kundu M., Dias J. C., Nunes-Pereira J., Botelho G., Silva M. M., Lanceros-Méndez S.: Mesoporous poly(vinylidene fluoride-*co*-trifluoroethylene) membranes for lithium-ion battery separators. Electrochimica Acta, **301**, 97–106 (2019).
https://doi.org/10.1016/j.electacta.2019.01.178

[48] Ghosh M., Vijayakumar V., Kurungot S.: Dendrite growth suppression by Zn^{2+}-integrated Nafion ionomer membranes: Beyond porous separators toward aqueous Zn/V$_2$O$_5$ batteries with extended cycle life. Energy Technology, **7**, 1900442 (2019).
https://doi.org/10.1002/ente.201900442

[49] Aziz S. B., Woo T. J., Kadir M. F. Z., Ahmed H. M.: A conceptual review on polymer electrolytes and ion transport models. Journal of Science: Advanced Materials and Devices, **3**, 1–17 (2018).
https://doi.org/10.1016/j.jsamd.2018.01.002

[50] Meng F., Gao J., Zhang M., Li D., Liu X.: Enhanced safety performance of automotive lithium-ion batteries with Al$_2$O$_3$-coated non-woven separator. Batteries and Supercaps, **4**, 146–151 (2021).
https://doi.org/10.1002/batt.202000169

[51] Janaum N., Butsiri T., Kasemsiri P., Souvanh M., Pongsa U., Theerakulpisut S., Hiziroglu S., Okhawilai M.: Multi response optimization of bioactive starch foam composite using Taguchi's method and Grey relational analysis. Journal of Polymers and the Environment, **28**, 1513–1525 (2020).
https://doi.org/10.1007/s10924-020-01706-x

[52] Datta S., Bandyopadhyay A., Pal P. K.: Grey-based Taguchi method for optimization of bead geometry in submerged arc bead-on-plate welding. The International Journal of Advanced Manufacturing Technology, **39**, 1136–1143 (2008).
https://doi.org/10.1007/s00170-007-1283-6